FINITE ELEMENT ANALYSIS OF SPOT LASER OF STEEL WELDING TEMPERATURE HISTORY

by

Khalid S. SHIBIB, Mohammed A. MINSHID, and Mayada M. TAHIR

Original scientific paper
UDC: 669.14:517.96:536.21
DOI: 10.2298/TSCI0904143S

Laser welding process reduces the heat input to the work-piece which is the main goal in aerospace and electronics industries. A finite element model for axi-symmetric transient heat conduction has been used to predict temperature distribution through a steel cylinder subjected to CW laser beam of rectangular beam profile. Many numerical improvements had been used to reduce time of calculation and size of the program so as to achieve the task with minimum time required. An experimental determined absorptivity has been used to determine heat induced when laser interact with material. The heat affected zone and welding zone have been estimated to determine the effect of welding on material. The ratio of depth to width of the welding zone can be changed by proper selection of beam power to meet the specific production requirement. The temperature history obtained numerically has been compared with experimental data indicating good agreement.

Key words: *laser spot welding, finite element model, welding zone, temperature history*

Introduction

The prediction of transient temperature distribution during welding process is important since the problem of distortion, residual stresses, grain structure, fast cooling, high temperatures, and reduced strength of material in and around weld joint result directly from the thermal cycle caused by the localized intense heat input [1]. The spot laser welding has many advantages over other welding process as it reduces the heat input to the work piece which is the main goal in aerospace and electronics industries. It also has higher efficiency, resulting in a smaller heat-affected-zone (HAZ) and applicability to heat sensitive material. By proper parameters selection the same devices may be used for laser welding or cutting. Due to these advantages, deep insight into this industrial process is needed.

Many researches have focused their research on this process [1-3], as shown here. Many of them is collected from experiments which simplify the solution for temperature history of spot laser welding. Computer program is created to predict the temperature distribution during the welding process. The Nd:YAG laser of wavelength 1.06 μm with rectangular beam profile was used to generate single spot welds on AISI 1006 steel cylinder having diameter and height of 10 mm .The schematic diagram which indicates the process is as shown in fig. 1.

An axi-symmetric finite element solution is obtained with a rectangular beam profile induced to 1 mm spot diameter focus at the surface also, by using a three-level scheme to avoid

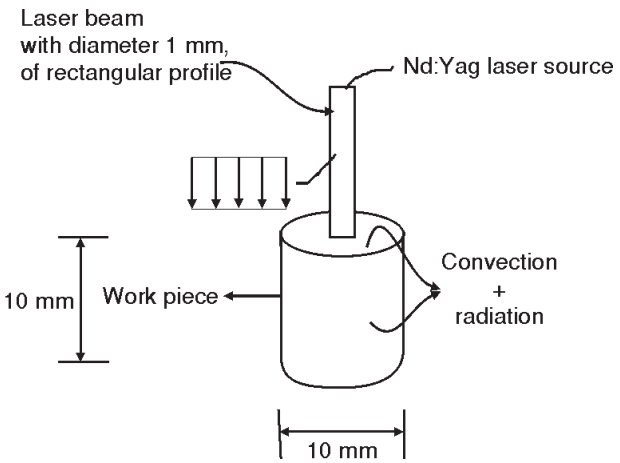

Figure 1. Schematic diagram of the laser welding process

iteration with convection and radiation at top and lateral surface. The finite element result is verified by comparing with the experimental data.

Theoretical model

Partial differential equation and boundary conditions

The equation of heat flow through a cylindrical steel specimen can be characterized by an axi-symmetric transient heat equation:

$$\rho c \frac{\partial T}{\partial t} \quad \frac{1}{r} \; k \frac{\partial}{\partial r} \quad r \frac{\partial T}{\partial r} \qquad k \frac{\partial^2 T}{\partial z^2} \quad \dot{Q} \tag{1}$$

As laser interacts with the metal surface a portion of the incident laser beam is absorbed and the rest is reflected. At low wave length this portion can be ignored for steel specimen, so that light intensity at any depth is:

$$q_z = q \exp(-\mu z) \tag{2}$$

where

$$q \quad \alpha \frac{P}{A} \tag{3}$$

Thus, the heat generation at any depth is:

$$\dot{Q} \quad \frac{\mathrm{d}q_z}{\mathrm{d}z} \quad q\mu \exp(\ \mu z) \tag{4}$$

where μ [m^{-1}]is the attenuation coefficient. For low carbon steel, μ is equal to 800 m^{-1}, as suggested by Mazumder *et al.* [2]. Material properties α and μ depend on laser wave length, nature of the surface, level of oxidization, surface temperature, beam power density, beam of incidence, and focal position of laser beam relative to work-piece surface.

Mazumder *et al.* [2] assumed that absorpitivity of the incident radiation below the boiling point is 20%. Frewin [3] also suggests that above boiling point 70% of the absorb radiation is further absorbed by vapor/plasma and the remaining 30% is transmitted through the vapor according to Beer-Lambert's law where it is fully absorb by the surface. An intense beam is focused on a small area which may rapidly raised the specimen temperature specially near the

surface which may melt and vaporize later on. A special attention should be paid to mesh refinement near the surface where laser beam continuously interacts with the material, in order to overcome solution instability and to take into account the accurate surface area that received laser photon. A fixed mesh is used and as a temperature of an element exceed boiling point its thermal properties will become that of material vapor (if known), and a latent heat of evaporation should be incorporated to account for evaporation.

The thermal properties are assumed to be temperature dependent and are taken from [4, 5]. Figure 2 shows the variation with temperature for thermal conductivity, specific heat, density, and emissivity.

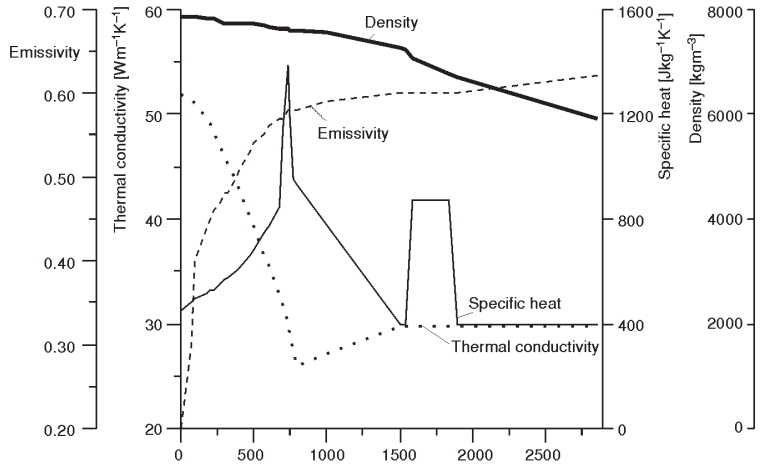

Figure 2. Thermal properties of AISI 1006 steel cylinder

An important change in thermal conductivity occurs at fusion temperature and liquid region was taken into account by the equation [6]:

$$k_{\text{eff}} = (1 - f)k_{\text{s}} + (1 + A_{\text{mix}})fk_{\text{l}} \tag{5}$$

where A_{mix} is the parameter describing the effect of solid convection (fluid motion) upon the thermal conductivity. If A_{mix} is zero, there is no increased heat transfer in the liquid region due to convection. The value of A_{mix} depends on the mixing intensity and for continuous steel casting process, A_{mix} values between 4 to 6 may be applied, as used in this work.

Single and efficient criteria for heat transfer coefficient, combining the radiation and convection from the welding process, can be used [7]:

$$h = 0.0026\,\varepsilon T^{1.6} \tag{6}$$

while the latent heat of fusion is simulated by an artificial increase in the liquid-specific heat according to Brown *et al*. [4].

Finite element formulation

The space-wise discretization of axi-symmetric heat equation can be accomplished using Galerkin method. If the volume of interest (domain) Ω is divided into a number of elements,

Ω^e, by using the usual shape function N_i, associated with each node, the unknown function T is approximated through the solution domain at any time by:

$$T = \Sigma N_i(r, z, t) T_i(t) \tag{7}$$

where $T_i(t)$ are the nodal parameters. Substitution of the above equation into the heat equation and by applying the Galerkin method results in a system of ordinary differential equations of the form [8]:

$$[C]\dot{\vec{T}} \quad [K]T \quad [F] \quad 0 \tag{8}$$

where $\dot{\vec{T}} \quad \begin{matrix} \frac{\partial T_1}{\partial t} \\ \frac{\partial T_2}{\partial t} \\ \\ \frac{\partial T_p}{\partial t} \end{matrix}$, $\vec{T} \quad \begin{matrix} T_1 \\ T_2 \\ .. \\ .. \\ T_p \end{matrix}$, $[\vec{F}] \quad \begin{matrix} F_1 \\ F_2 \\ .. \\ F_p \end{matrix}$ and p is the total number of nodes.

The typical matrices of elements are:

$$K_{ij} \quad k \frac{\partial N_i}{\partial r}\frac{\partial N_j}{\partial r} \quad k \frac{\partial N_i}{\partial r}\frac{\partial N_j}{\partial r} \quad d\Omega \quad N_i h d\Gamma \tag{9}$$

$$C_{ij} \quad \rho C N_i N_j \, d\Omega \tag{10}$$

$$F_i \quad N_i(Q \quad hT_\infty) d\Gamma \quad N_i \dot{Q} d\Omega \tag{11}$$

The summation are taken over the contribution of each element, Ω^e, in the element volume and Γ^e refers only to the element with external boundary on which surface condition is applied. To avoid iteration at each time step, the unconditionally stable three-level scheme proposed by Lees [8], is used here resulting in:

$$\frac{3[C_n]}{2\Delta t} \quad [K_n] \quad \vec{T}_{n\ 1} \quad [K_n]\vec{T}_n \quad [K_n]\vec{T}_{n\ 1} \quad \frac{3}{2\Delta t}[C_n]\vec{T}_{n\ 1} \quad 3\vec{F} \tag{12}$$

In the solution process the well-known method suggested by Comini [8] is used. The values of matrices at the intermediate time are sufficient to solve the simultaneous equations at each time step .The values of the temperature at the end of the total three level are replaced to be the intermediate values for the next time step two starting values of the temperature distribution can assumed to start the solution of eq. (12). The efficient procedure of solving the equations by avoiding time consuming procedure of iteration is combined with band solver matrix solution dramatically reducing the time of calculation and the size of the program.

Result and discussion

Classification of results needs a definition of welding zone (WZ), including HAZ, where the temperature is higher than 730 °C, plus fusion zone (FZ), where the temperature is higher than 1540 °C.

Figure 3 represents domain dimensions and the used mesh. Only one-half of the cross-section is drawn because of symmetry. Also in fig. 3, the location of thermocouple (type J) used to compare the theoretical result with the experimental one, is indicated.

Figure 4 indicates temperature distribution for laser power 1 kW. When the depth of FZ reaches 0.7 mm the laser power is cut-off. The time required to reach this temperature at specified depth is 0.11 s for 1 kW and 0.0192 s for 2 kW. The benefit of using rectangular beam shape is to distribute a constant power flux over the entire area of the spot, which results in a wider spot area comparing with that of Gaussian distributed beam (see ref. [3]).

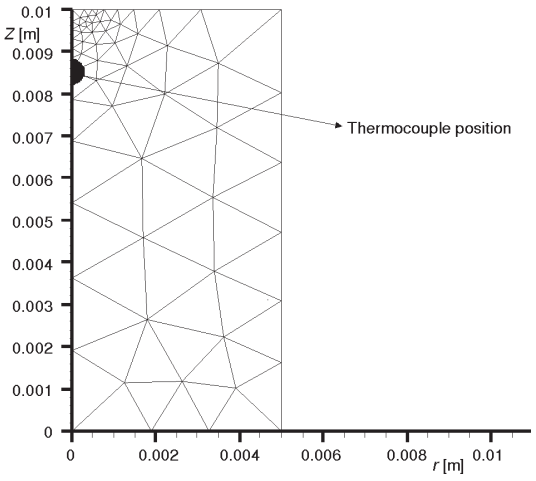

Figure 3. Dimensions, mesh, and thermocouple position for a specimen

Figure 5 indicates temperature distribution for laser beam power of 2 kW where the increase in laser power results in a deeper FZ comparing with that of width, but shorter time is required to achieve the task (*i. e.* to reach the temperature of 1540 °C at $Z = 9.3$ mm), tabs. 1 and 2.

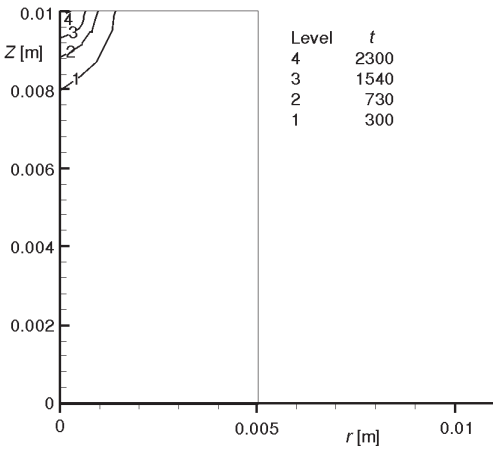

Figure 4. Temperature distribution at the end of laser exposed at time of 0.11 s for laser power 1 kW

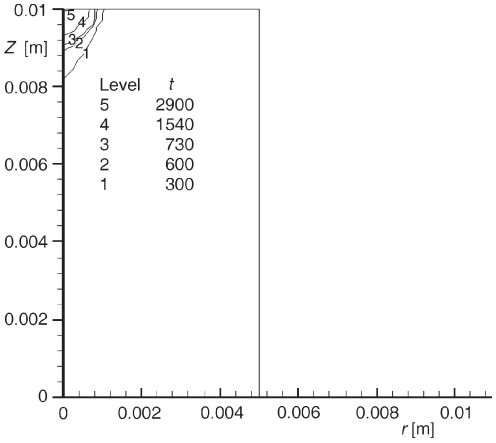

Figure 5. Temperature distribution at the specimen where laser power 2 kW, cut-off time 0.0195 s

Table 1. Depth of FZ and WZ *vs.* laser power

1 kW	2 kW	T [°C]
0.7 mm	0.7 mm	1540
1.15 mm	1.04 mm	730
2 mm	1.77 mm	300

Table 2. Ratio of width to depth *vs.* laser power

1 kW	2 kW	T [°C]
2.1	1.96	1540
1.714	1.7	730
1.4	1.16	300

A slightly larger ratio of width to depth for FZ and WZ is obtained as laser power is reduced even if the same radius is used for the laser beam. The depth of FZ and HAZ for lower laser power is larger, because longer time had been used to expose the specimen. Also the temperature at depth of 0.7 mm equals to 1540 °C at both power level, the depth of WZ for laser power of 1 kW being larger, which means as power increased the depth of welding zone can be reduced, if the goal is to reach fusion temperature at a depth of 0.7 mm, as clearly shown in tabs. 1 and 2 and figs. 4 and 5. A choice may be taken by the demand of the spot welding type necessary to achieve special requirement presented by the whether the deeper spot welding is needed or a wider one.

Figure 5 indicates temperature distribution after 1 second where a combined radiation and convection heat transfer coefficient is used to determine the heat transfer through the surface (top and lateral). A high thermal conductivity at moderate temperature will lead to rapid diffusion of heat through the sample and this influence combined with the effect of heat loss due to convection and radiation will cause a rapid decrease in temperature distribution, as shown in fig. 6.

Finally, a simple verification of the mathematical method is used. A thermocouple type J is inserted in a location indicated by a small semi-circular shown in fig. 3. The result obtained from the mathematical model is shown in fig. 6, being in good agreement with the experimental results, also shown in fig. 7, which verifies the proposed method of solution used here.

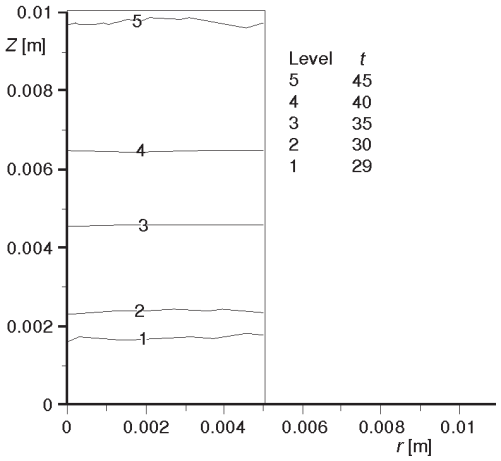

Figure 6. Temperature distribution in specimen after 1 s for laser power of 1 kW

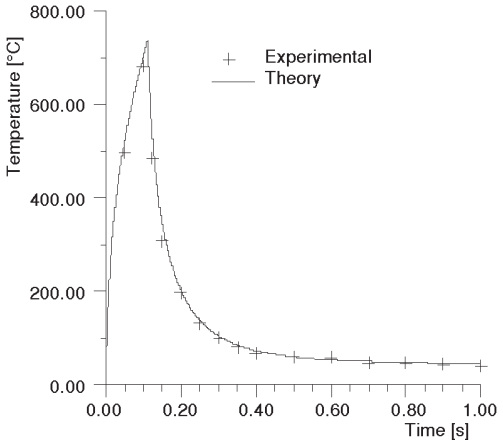

Figure 7. Experimental and theoretical temperature history on position that had been exist at axis of symmetry and Z = 8.7 mm for laser power of 1 kW

Conclusions

Based on the results presented in this paper the following conclusions can be drawn.

The finite element had been used successfully to predict temperature distribution through a steel specimen during spot laser welding process. A three-level scheme had been used to avoid time consuming scheme of iteration, combined with band solver matrix technique to minimize time required to achieve the calculation and the size of program. The results between experimental and numerical temperature distribution are in good agreement.

The spot laser welding process with two power levels has been tested to show their effect on size of spot in width and depth. For certain depth of welding required, a low laser power may result in a deeper HAZ with high width to depth ratio comparing with that of high power.

Nomenclature

A – area, [m^2]
c – specific heat, [Jkg^{-1}K^{-1}]
f – area fraction
h – heat transfer coefficient, [Wm^{-2}K^{-1}]
k – thermal conductivity, [Wm^{-2}K^{-1}]
N – shape function
P – power, [W]
Q – heat flux, [Wm^{-2}]
$\dot{Q}$ – heat generation, [Wm^{-3}]
q – light intensity, [Wm^{-2}]
r – radial dimension, [m]
T – temperature, [°C]
t – time, [s]
z – axial dimension, [m]
[K],[C],[F] – matrices

Greek letters

α – absorptivity
ε – emissivity
μ – attenuation coefficient, [m^{-1}]
ρ – density, [kgm^{-3}]
Γ – surface
Ω – volume

Subscripts

eff – effective
l – liquid
n–1, n, n+1 – time steps
s – solid
z – depth
∞ – environmental

References

[1] Goldak, J. A., Chakravarti, A. P., Bibby, M., A New Finite Element Model for Welding Heat Source, *Metallurgical and Materials Transaction B, 15* (1984), 2, pp. 299-305
[2] Mazumder, J., Steen, W. M., Heat Transfer Model for CW Laser Material Processing. *J. Appl.Phys., 51* (1980), 2, pp. 941-947
[3] Frewin, M. R., Scott, D. A., Finite Element Model of Pulsed Laser Welding, *Welding J. Research Supplement, 78* (1999), 1, pp. 15-22
[4] Brown, S., Song, H., Finite Element Simulation of Welding of large Structures. *J. Eng. Ind., 114* (1991), 11, pp. 441-451
[5] Kim, C. S., Thermo Physical Properties of Stainless Steels, Technical Report ANL-75-55, Argonne National Laboratory, Argonne, Ill., USA, 1975, pp. 1-24
[6] Miettinen, J., Louhenklipi, Calculation of Thermo Physical Properties of Carbon and Low Alloyed Steels for Modeling of Solidification Processes, *Metallurgical and Materials Transactions, 25* (1994), 6, pp. 909-916
[7] Vinokurov, V. A., Welding Stresses Distortion, The British Library, Boston Spa, England, 1977, pp. 108-110
[8] Lewis, R. W., *et al*., The Finite Element Method in Heat Transfer Analysis, John Wiley & Sons Ltd., Chichester, UK, 1996

Authors' affiliation:

K. S. Shibib (**correspondin author**)
University of Technology Baghdad
Department of Laser and Optoelectronics Engineering
P.O Box 35010
Baghdad, Iraq
E-mail: Assprofkh@coolgoose.com

M. A. Minshid, M. M. Tahir
University of Technology Baghdad
Department of Laser and Optoelectronics Engineering
Baghdad, Iraq

Paper submitted: July 16, 2008
Paper revised: January 24, 2009
Paper accepted: March 21, 2009